Journal of Physics B: Atomic, Molecular and Optical Physics

PAPER • OPEN ACCESS

Terahertz magnetic field enhancement in an asymmetric spiral metamaterial

To cite this article: Debanjan Polley *et al* 2018 *J. Phys. B: At. Mol. Opt. Phys.* **51** 224001

OPEN ACCESS
IOP Publishing
Journal of Physics B: Atomic, Molecular and Optical Physics
J. Phys. B: At. Mol. Opt. Phys. **51** (2018) 224001 (8pp)
https://doi.org/10.1088/1361-6455/aae579

Terahertz magnetic field enhancement in an asymmetric spiral metamaterial

Debanjan Polley[1], Nanna Zhou Hagström[1,2], Clemens von Korff Schmising[2], Stefan Eisebitt[2,3] and Stefano Bonetti[1]

[1] Department of Physics, Stockholm University, SE-106 91 Stockholm, Sweden
[2] MBI Max-Born Institute for Nonlinear Optics and Short Pulse Spectroscopy, Max-Born-Str. 2A, D-12489 Berlin, Germany
[3] Institut fr Optik und Atomare Physik, Technische Universität Berlin, D-10623 Berlin, Germany

E-mail: stefano.bonetti@fysik.su.se

Received 26 June 2018, revised 4 September 2018
Accepted for publication 1 October 2018
Published 25 October 2018

Abstract

We use finite element simulations in both the frequency and the time-domain to study the terahertz resonance characteristics of a metamaterial (MM) comprising a spiral connected to a straight arm. The MM acts as a RLC circuit whose resonance frequency can be precisely tuned by varying the characteristic geometrical parameters of the spiral: inner and outer radius, width and number of turns. We provide a simple analytical model that uses these geometrical parameters as input to give accurate estimates of the resonance frequency. Finite element simulations show that linearly polarized terahertz radiation efficiently couples to the MM thanks to the straight arm, inducing a current in the spiral, which in turn induces a resonant magnetic field enhancement at the center of the spiral. We observe a large (approximately 40 times) and uniform (over an area of $\sim$10 μm^2) enhancement of the magnetic field for narrowband terahertz radiation with frequency matching the resonance frequency of the MM. When a broadband, single-cycle terahertz pulse propagates towards the MM, the peak magnetic field of the resulting band-passed waveform still maintains a six-fold enhancement compared to the peak impinging field. Using existing laser-based terahertz sources, our MM design allows to generate magnetic fields of the order of 2 T over a time scale of several picoseconds, enabling the investigation of nonlinear ultrafast spin dynamics in table-top experiments. Furthermore, our MM can be implemented to generate intense near-field narrowband, multi-cycle electromagnetic fields to study generic ultrafast resonant terahertz dynamics in condensed matter.

Keywords: terahertz, magnetic field, metamaterials

(Some figures may appear in colour only in the online journal)

1. Introduction

With the advances in the development of laser-based, table-top sources [1–4], strong terahertz radiation has become a novel tool to investigate low-energy excitations in condensed matter physics [5–11]. Within the very active research field of ultrafast magnetism, sub-ps demagnetization dynamics in metallic films triggered by single-cycle terahertz radiation have been observed [12–15]. Compared to the near-infrared lasers more commonly used in this type of experiments [16–19], terahertz radiation, via its magnetic field component, can couple directly to the spin degree of freedom, rather than through thermalization of highly energetic excited states. For instance, with single-cycle terahertz magnetic fields of the order of 1 T, it is possible to induce coherent precessional or 'ballistic' magnetization reversal in a metallic ferromagnet [20–22]. To date, it is still difficult to generate such a strong terahertz magnetic field with table-top sources and, so far,

only accelerator-based sources have been able to achieve a precessional magnetization reversal.

In the last few years, the enhancement of the terahertz *electric* field using metamaterials (MMs) has been realized using several methods [23–26]. However, only few works have been addressing the enhancement of the *magnetic* counterpart [27–30]. MMs have long been studied for their exotic tunable electromagnetic response unavailable in naturally occurring materials [31–36]. Split-ring resonators [28, 37] are one class of MMs in which an enhancement of the magnetic field due to the an eddy current circulating around the MM has been observed [27, 28, 38–40]. While the magnetic field is indeed strongly enhanced, such an enhancement is mostly concentrated on the edges of the MM, and remains small in the central gap of the MM. Only very recently, a combination of MM and a complex three-dimensional tapered waveguide has been used to increase the terahertz magnetic field more uniformly [30]. We have also recently shown that, by introducing an asymmetric arm in a circular split-ring resonator, a relatively easily fabricated structure, the terahertz magnetic field can be enhanced tenfold in the central gap of the MM, while the corresponding electric field enhancement remained small [29].

In this work, we go beyond our previous study [29] by thoroughly investigating the design of an asymmetric spiral split-ring resonator that greatly enhances the magnetic component of the terahertz radiation, while only slightly enhancing the electric field component. We use finite element simulations in both the frequency- and the time-domain to investigate the three-dimensional distribution of electric and magnetic fields in such a structure. The MM, which can be described in terms of a resonant RLC circuit, is optimized to maximize the enhancement at 1 THz, roughly the center frequency of the 2 THz bandwidth of the radiation generated with well-established table-top laser-based terahertz sources. The optimized design shows a much larger enhancement compared to our previous work. We also present an analytical model that can be used to calculate the resonance frequency of the MM when the inner and outer radii, the width and the number of turns of the structure are varied. Finally, we find that finite element simulations in the time domain are necessary to reveal the complex evolution of the electromagnetic field in the MM, and to correctly estimate the peak-field enhancement with respect to an incoming broadband, single-cycle terahertz source.

2. MM structure

We use the full three-dimensional finite-element method implemented in the Wave Optics module of the COMSOL Multiphysics software [41] to study the near-field enhancement of the THz electric and magnetic fields in both time and frequency domains in a resonant asymmetric spiral MM structure shown schematically in figure 1(a).

The unit cell of the MM is a 200 nm thick spiral asymmetric gold split-ring-resonator, on top of a $t = 150$ μm thick glass substrate. The structure also includes adjacent blocks of air with thickness 300 μm (the vacuum wavelength of electromagnetic radiation with frequency of 1 THz) on top of the gold structure, and at the bottom of the glass substrate. We chose these thickness in order to fulfill the condition of layers with minimum dimensions of the order λ_0/n, where λ_0 is the wavelength of the radiation in vacuum. We used $P_x = 60$ μm and $P_y = 52$ μm for the lateral sizes of the unit cell. For the frequency-domain simulations, perfectly matched layers with thickness $\lambda_0/5$ are used at the top and the bottom boundaries of the simulation region to get rid of the unwanted reflections of the electromagnetic waves. In the time-domain simulation, the same effect is achieved implementing scattering boundary conditions. Perfect magnetic conductor and perfect electric conductor boundary conditions are applied to the surfaces parallel to the xz and yz planes, respectively, since the radiation is linearly polarized with the electric field along x. The gold MM has a minimum tetrahedral mesh size of approximately 13 nm. The substrate and the air blocks are divided into tetrahedral meshes with a minimum mesh size of about 0.5 μm and maximum mesh size of $\lambda_0/(20n)$. For the substrate, we used the experimental value $\epsilon_r = n^2 = 3.84$ for the relative permittivity [42]. The metallic Au layer is modeled as a lossy metal with the frequency-independent conductivity of gold, $\sigma = 4.09 \times 10^7$ Sm^{-1} [43].

In order to systematically control the shape of the MM, we use the following parametric equation for an Archimedean spiral

$$x = (r + b\theta)\cos\theta, \quad (1)$$

$$y = (r + b\theta)\sin\theta, \quad (2)$$

with $b = (r_{out} - r_{in})/2\pi N$ and $\theta = 2\pi N$, in order to draw the structure as a function of three parameters: outer radius (r_{out}), inner radius (r_{in}), number of turns (N), indicated in figure 1(a). The fourth parameter, the width (w) of the conductor line, can be set by drawing two spirals of radius differing by an amount equal to w. Finally, a rectangular arm with length l and width w is added to the spiral structure. The function of this straight arm is to efficiently couple linearly polarized electromagnetic radiation impinging perpendicular to the plane of the structure, and with the magnetic field perpendicular to the arm. The screening of the *magnetic* field component orthogonal to the arm induces an eddy current parallel to the long side of the arm. Such current flows inside the spiral, which then simply acts as a solenoid where the magnetic field adds up constructively. We highlight the critical importance of this arm to effectively couple the linearly polarized terahertz radiation with the MM structure. As discussed in previous works [29, 36], we also stress that the electric field component is screened very effectively at the gold surface. Typical terahertz electric fields generated with table-top sources (up to 100 MV m^{-1}, 1 ps in duration) are screened by a slight rearrangement of the surface charges within the first atomic layer within the metal. These charges react on the femtosecond time scale, and are subjected to interatomic electric fields more than two order of magnitude larger than the impinging terahertz field. Hence, inside the conductor, the magnetic field component of the radiation is much larger than the electric field component [44]. More precisely, the relative ratio of

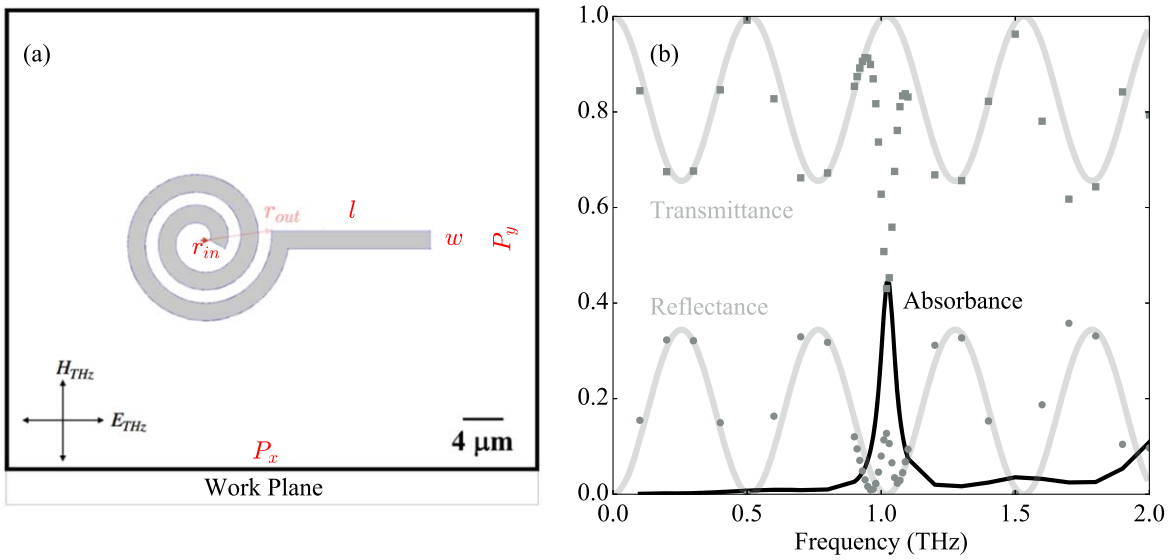

Figure 1. (a) Top view of the work plane, the parameters of the MM are $P_x = 60$ μm, $P_y = 52$ μm, $r_{out} = 8$ μm, $r_{in} = 1$ μm, $n = 2$, $l = 18$ μm, $w = 2$ μm, (b) simulated transmittance (square symbols), reflectance (round symbols) and absorbance (solid black line) of the MM as a function of incident THz frequency. The semi-transparent line is the expected variation of transmittance and reflectance from the analytical etalon equation described in the main text.

their modules squared compared to their ratio in vacuum is equal to the dielectric constant of the metal, assuming $\mu_r = 1$. This assumption on the relative permeability is generally true, even (in the terahertz range) for magnetic conductors.

3. Resonance frequency

We performed full three-dimensional finite element simulations in the frequency domain in the range 0.1–2.0 THz. Near the resonance frequency, between 0.9 and 1.1 THz the frequency step is set to 0.01 THz, while in the rest of the frequency range we used a frequency resolution of 0.1 THz. The present MM structure is optimized for maximum terahertz field enhancement around 1.0 THz, which is in proximity of the center of the bandwidth of commonly used broadband table-top THz sources [45–49]. For the geometrical parameters given in the caption of figure 1, the transmittance (T), reflectance (R), and absorbance (A) all exhibit a sharp features at 1.02 THz, as shown in figure 1(b). The absorption peak has a maximum value of approximately 44%, clearly indicating the activation of the MM response at resonance. The reflectance and transmittance spectra, in addition to the resonance feature, show clear Fabry–Perot oscillations due to the finite glass thickness. The oscillations can be accurately described using nominal parameters in the formulas $R = |E|^2 \sin^2(2\pi\nu/\nu_0)$, and $T = 1 - |E|^2 \sin^2(2\pi\nu/\nu_0)$, with $\nu_0 = c/nt$, where c is the speed of light in vacuum, and $E = (1/n - n)/(n + 1/n)$ is the maximum reflection for an etalon, using only nominal parameters.

By varying the MM geometrical parameters, the resonance frequency can be tuned [50–52]. We have studied such frequency tuning, specifically its dependence on the four variables that parameterize the spiral. We varied each one of these variables, time while keeping the other three fixed at the values reported in the caption of figure 1. The solid symbols plotted in the four panels of figure 2 show the simulated resonance frequency of the MM as a function of the variable reported in the x-axis. The general trend is the decrease of resonance frequency with increasing structure size. For these plots, the reported frequency is accurate within 0.1 THz, which correspond to the frequency step size of the finite element numerical simulations.

While these numerical simulations are very accurate in predicting the correct resonance frequency and enhancement, they are also computationally very demanding. Each simulated point took ~10 h on a 40-core workstation with 128 GB of RAM, making the design from scratch of an arbitrary structure unpractical. For this reason, we explored the possibility of using an analytical model to describe the dependence of the resonance frequency on the four geometrical variables. A resonant MM can in general be described as a RLC circuit where the R, L and C are the inductance, capacitance and resistance, respectively, of an equivalent circuit model of the structure. The resonance frequency of such a circuit would then be $f = 1/2\pi\sqrt{LC}$, where the inductance L and the capacitance C of a spiral are approximated with the expressions valid for concentric coils [53] and, respectively, for a solenoid [54]:

$$L = \frac{\mu_r \mu_0}{2\pi}\left[\frac{(ND/2)^2}{100(2D + 5.3(r_{out} - r_{in}))}\right], \tag{3}$$

$$C = \frac{4\epsilon_r \epsilon_0}{\pi} l\left[1 + 0.71\left(\frac{D}{l}\right) + 2.40\left(\frac{D}{l}\right)^{\frac{3}{2}}\right], \tag{4}$$

where μ_0 and ϵ_0 are the vacuum permeability and permittivity, and μ_r and ϵ_r are the relative permeability and permittivity of the effective medium. D and l are the average diameter and, respectively, total length of the spiral. The length of an Archimedean spiral is

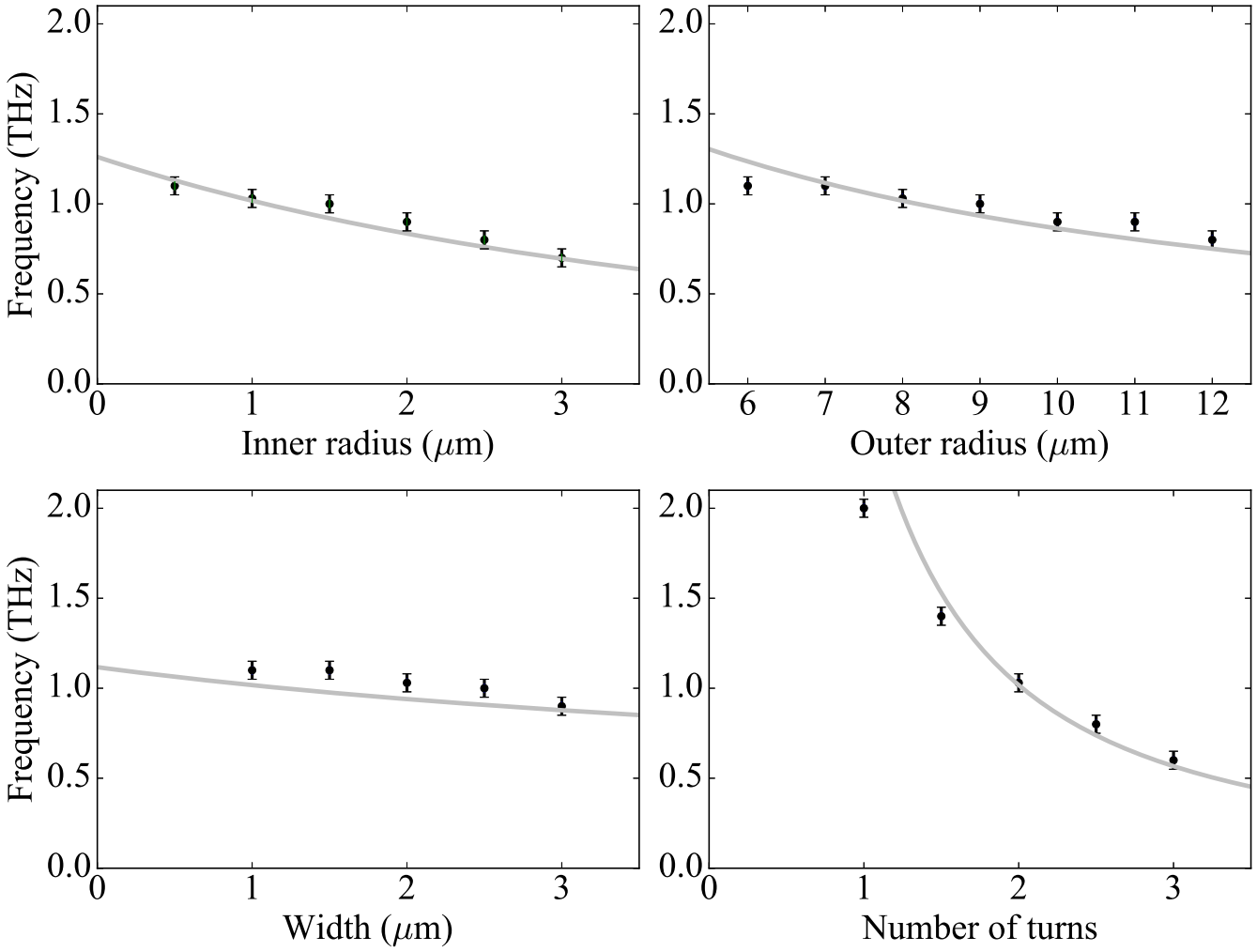

Figure 2. The dependence of the resonance frequency on the structure parameters of the MM namely (a) inner radius (r_{in}), (b) outer radius r_{out}, (c) width (w) and (d) number of turns (N) of the metamaterial. The errorbars have a constant value equal to half of the frequency step used in the calculations. The continuous line is the expected resonance frequency calculated with the analytical model described in the text.

$$l = \int_0^{2\pi N} \sqrt{r^2 + \left(\frac{dr}{d\theta}\right)^2}\, d\theta, \tag{5}$$

where r is the radius of the spiral.

By scaling the resonance frequency with a single parameter c, we rewrite the equation for the resonance frequency of the spiral as

$$f_s = \frac{c}{2\pi\sqrt{LC}}. \tag{6}$$

The predicted resonance frequencies for the analytical model are plotted as the gray solid line in figure 2. Assuming the single value $c \approx 1.54$, the analytical equations reproduce well the resonance frequency of the MM as a function of each of the four geometrical variables. A correction factor c is to be expected, as our spiral is only an approximation of the concentric coil or of the solenoid modeled by equations (3) and (4). This discrepancy is particular evident for the case when the number of turns is lowest, i.e. for $N = 1$, when the approximation of our coil with a solenoid is least accurate.

The resistance of the MM can be computed in a straightforward way as $R = \rho l/wt$, where ρ is the resistivity of the metal used for the MM, and t its thickness. The full-width half-maximum bandwidth of the resonance is then $\Delta f = 2\pi R/L$, which returns the correct order of magnitude $\Delta f \approx 0.1$ THz for $r_{out} = 8$ μm, $r_{in} = 1$ μm, $N = 2$, $l = 18$ μm, $w = 2$ μm, i.e. for the coil plotted in figure 1(a), as evident in the absorbance of plot of figure 1(b) and as confirmed by the time-domain simulations discussed below.

4. Field enhancement

In order to compute the enhancement of the electric and magnetic field components of the terahertz radiation, we performed finite element simulations both in the frequency and the time domain. The frequency domain results allow to draw a two-dimensional 'enhancement map' in the region surrounding the MM. The time-domain computations return the detailed temporal evolution of the electric and magnetic fields at a given point in space. The time-domain simulations are particularly relevant for experiments where broadband, single-cycle terahertz pulses are used to excite dynamics in materials. In the following, we assume the MM structure

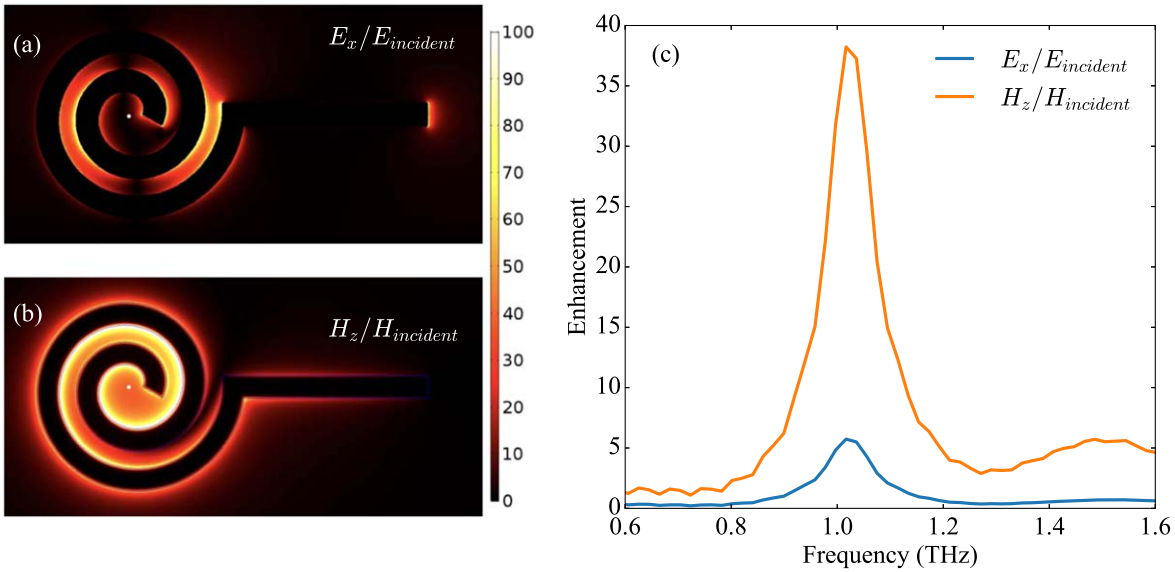

Figure 3. The (a) electric and (b) magnetic field enhancement (with respect to the incident field) at the MM plane observed from the frequency domain analysis. The enhancement observed by Fourier transforming the time domain data from figure 4 is shown in (c). The white dot in (a) and (b) is the origin of the spiral, where the enhancement in the time domain simulation is calculated.

plotted in figure 1(a), with the dimensions reported in the respective caption.

For the frequency domain analysis, we have used an approach similar to our earlier work to calculate the enhancement factor [29]. Briefly, the terahertz electric $E_{incident}$ and magnetic $H_{incident}$ fields (assumed to be uniform over the sample plane) incident on the MM are taken as reference. Once the terahertz electric E_x and magnetic H_z field values at the MM surface are determined, they are normalized by the incident fields to determine the enhancement factor. We chose the x and z component of the electric and magnetic fields, respectively, as they are the ones most strongly enhanced by the MM structure discussed here.

The enhancement maps for the electric and the magnetic fields at the MM surface are the plotted in figure 3(a) and, respectively, figure 3(b) using the same color scale. The magnetic field enhancement is moderately uniform over the central gap, and it is much larger than the electric field enhancement. Furthermore, the electric field is mostly enhanced in the outer annular region and in the outer edge of the spiral MM, and it is only slightly enhanced in the central gap of the spiral. This is more evidently shown in figure 3(c), where we plot the enhancement factor at the center of the spiral in the region indicated by the white dot in figures 3(a) and (b). The curves in figure 3(c) are the Fourier transform of the simulated time-domain traces discussed below. It can be clearly seen that the electric field enhancement is a factor of about 5, while the magnetic field enhancement reaches almost a factor of 40.

We now turn to the time-domain simulations. In this case, we used as the reference field the electric field of a typical broadband, single-cycle terahertz pulse measured experimentally in our laboratory using electro-optical sampling in a GaP crystal. The terahertz electric field is plotted as the semi-opaque line in figure 4(a), with a peak of approximately 1 MV cm^{-1}. The corresponding peak magnetic field has a value of 0.33 T. These are the typical field values nowadays attainable with state-of-the-art laser-based terahertz sources. In figures 4(a) and (b) we plot the calculated enhancement of the x component of the electric field and, respectively, of the z component of the magnetic field at the center of the spiral. The most striking feature for both field components is that the single-cycle, broadband incident field has now the shape of a damped narrowband oscillation at a frequency of approximately 1 THz. This is not surprising considering the narrow resonance of the structure plotted in figure 1(b). It is however worth highlighting that the broadband characteristics of the pulse can be preserved in other types of MM structures, when the resonance frequency is far off the bandwidth of the impinging radiation [36, 55].

Considering the field enhancement, the MM structure does not substantially modify the peak value of the electric field component, as compared to the incident field and as shown in figure 4(a). On the other hand, the magnetic field component of the radiation is enhanced by a factor of roughly 6, reaching peak values of approximately 2 T. The apparent discrepancy in the simulated enhancement factor between the frequency-and the time-domain simulations is readily explained. The peak-field enhancement in the time-domain is the overall, broadband enhancement. Conversely, the frequency-domain analysis returns the enhancement factor at a single frequency. In order to confirm the consistency between the two simulations in the reciprocal domains, we note that the expected enhancement at the resonance frequency is the same for both frequency domain simulations plotted in figures 3(a), (b), and the one computed by Fourier transform of the time-domain trace, shown in figure 3(c).

Finally, the time-domain simulations demonstrate that our MM structure can be used not only to enhance the magnetic field component of incident terahertz radiation, but

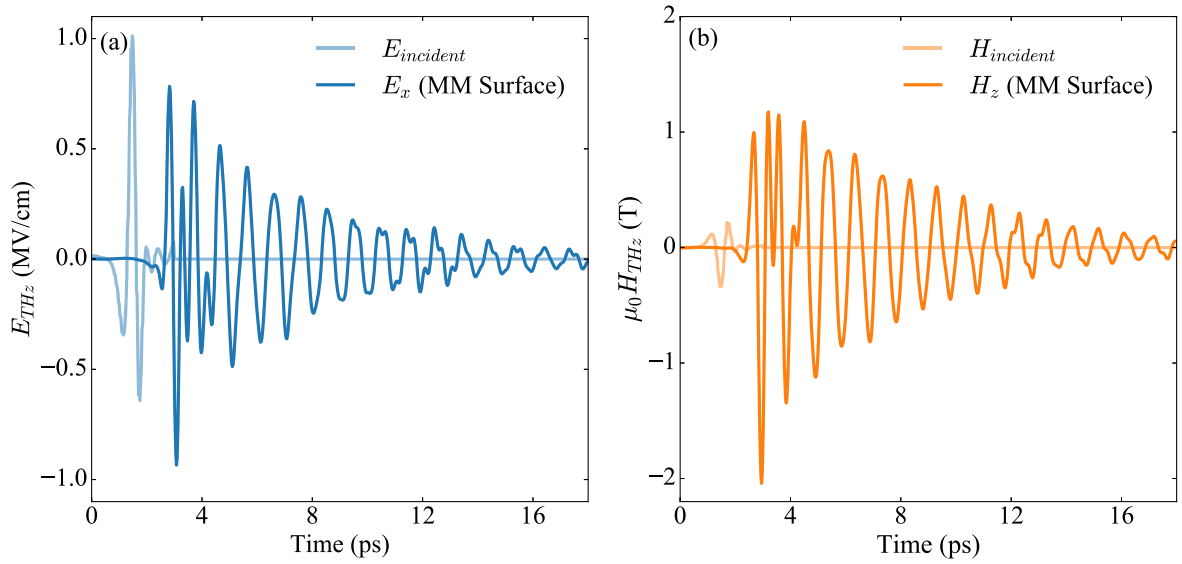

Figure 4. The (a) electric (E_y) and (b) magnetic field (H_z) profile at the origin of the spiral MM as obtained from the time-domain simulation. The incident electric $E_{incident}$ and magnetic $H_{incident}$ fields are shown in semi-transparent color between 0 and 3 ps.

more generally to generate intense narrowband, multi-cycle terahertz pulses starting from broadband ones. While broadband terahertz radiation is nowadays commonly generated with table-top lasers, narrowband radiation is still relatively challenging to achieve in these systems [56–59], and accelerator-based sources are needed [60, 61]. With our MM design, intense electric (1 MV cm^{-1}) and magnetic (2 T) narrowband terahertz fields become accessible in small-scale laboratories.

5. Conclusion

We have used finite element method simulations in both the frequency and the time domain to compute the near-field enhancement in a planar, asymmetric spiral MM structure. We designed the MM to provide resonant enhancement at around 1 THz, roughly at the center frequency of the broadband terahertz radiation generated with state-of-the-art laser-based sources. We have shown that the dependence of the resonance frequency on the geometrical parameters of the structure can be accurately predicted by a simple analytical model that describes the MM structure as a resonant RLC circuit.

Numerical simulations have shown large enhancement of the terahertz magnetic field (40-fold at the resonant frequency, six-fold over the broadband), and negligible electric field enhancement (five-fold at the resonant frequency, no enhancement over the broadband). This is at times desirable, as strong electric fields can cause dielectric breakdown and be potentially damaging for solid state experiments. The magnetic field enhancement is quite uniform over a $\sim$10 μm^2 region at the center of the spiral. Additionally, our MM can be used as a table-top near-field source of narrowband, multi-cycle terahertz radiation driven by broadband terahertz pules. The peak fields achievable (electric field: 1 MV cm^{-1}, magnetic field: 2 T) are large enough to induce nonlinear effects in solids.

We envision that our MM will open up new possibilities for experiments of ultrafast nonlinear spin dynamics in different ferromagnetic and antiferromagnetic systems. We also anticipate that our simple MM design will enable the broad investigation of resonant and nonlinear terahertz dynamics of electrons, phonons and magnons in table-top experiments.

Acknowledgments

We are grateful to Matteo Pancaldi for the support with COMSOL simulations, and to Paolo Vavassori and Ioan Tudosa for fruitful discussion on the interaction between matter and electromagnetic radiation. DP and SB acknowledge support from the European Research Council, Starting Grant 715452 MAGNETIC-SPEED-LIMIT.

ORCID iDs

Stefano Bonetti https://orcid.org/0000-0001-9352-2411

References

[1] Taniuchi T, Okada S and Nakanishi H 2004 Widely tunable terahertz-wave generation in an organic crystal and its spectroscopic application *J. Appl. Phys.* **95** 5984–8
[2] Houard A, Liu Y, Prade B, Tikhonchuk V T and Mysyrowicz A 2008 Strong enhancement of terahertz radiation from laser filaments in air by a static electric field *Phys. Rev. Lett.* **100** 255006
[3] Hauri C P, Ruchert C, Vicario C and Ardana F 2011 Strong-field single-cycle THz pulses generated in an organic crystal *Appl. Phys. Lett.* **99** 161116

[4] Wu X, Carbajo S, Ravi K, Ahr F, Cirmi G, Zhou Y, Mücke O D and Kärtner F X 2014 Terahertz generation in lithium niobate driven by ti:sapphire laser pulses and its limitations *Opt. Lett.* **39** 5403–6

[5] Hoffmann M C, Brandt N C, Hwang H Y, Yeh K-L and Nelson K A 2009 Terahertz kerr effect *Appl. Phys. Lett.* **95** 231105

[6] Kampfrath T, Sell A, Klatt G, Pashkin A, Mährlein S, Dekorsy T, Wolf M, Fiebig M, Leitenstorfer A and Huber R 2011 Coherent terahertz control of antiferromagnetic spin waves *Nat. Photon.* **5** 31

[7] Dienst A, Hoffmann M C, Fausti D, Petersen J C, Pyon S, Takayama T, Takagi H and Cavalleri A 2011 Bi-directional ultrafast electric-field gating of interlayer charge transport in a cuprate superconductor *Nat. Photon.* **5** 485

[8] Hu W, Kaiser S, Nicoletti D, Hunt C R, Gierz I, Hoffmann M C, Tacon M L, Loew T, Keimer B and Cavalleri A 2014 Optically enhanced coherent transport in $YBa_2Cu_3O_{6.5}$ by ultrafast redistribution of interlayer coupling *Nat. Mater.* **13** 705

[9] Li S, Kumar G and Murphy T E 2015 Terahertz nonlinear conduction and absorption saturation in silicon waveguides *Optica* **2** 553–7

[10] Shalaby M, Vicario C and Hauri C P 2017 Extreme nonlinear terahertz electro-optics in diamond for ultrafast pulse switching *APL Photonics* **2** 036106

[11] Woldegeorgis A, Kurihara T, Beleites B, Bossert J, Grosse R, Paulus G G, Ronneberger F and Gopal A 2018 Thz induced nonlinear effects in materials at intensities above 26 gw/cm2 *J. Infrared Millim. Terahertz Waves* **39** 667–80

[12] Vicario C, Ruchert C, Ardana-Lamas F, Derlet P M, Tudu B, Luning J and Hauri C P 2013 Off-resonant magnetization dynamics phase-locked to an intense phase-stable terahertz transient *Nat. Photon.* **7** 720

[13] Bonetti S, Hoffmann M C, Sher M-J, Chen Z, Yang S-H, Samant M G, Parkin S S P and Dürr H A 2016 Thz-driven ultrafast spin-lattice scattering in amorphous metallic ferromagnets *Phys. Rev. Lett.* **117** 087205

[14] Shalaby M, Vicario C and Hauri C P 2016 Simultaneous electronic and the magnetic excitation of a ferromagnet by intense thz pulses *New J. Phys.* **18** 013019

[15] Shalaby M, Vicario C and Hauri C P 2016 Low frequency terahertz-induced demagnetization in ferromagnetic nickel *Appl. Phys. Lett.* **108** 182903

[16] Beaurepaire E, Turner G M, Harrel S M, Beard M C, Bigot J-Y and Schmuttenmaer C A 2004 Coherent terahertz emission from ferromagnetic films excited by femtosecond laser pulses *Appl. Phys. Lett.* **84** 3465–7

[17] Koopmans B, Van Kampen M, Kohlhepp J T and De Jonge W J M 2000 Ultrafast magneto-optics in nickel: magnetism or optics? *Phys. Rev. Lett.* **85** 844

[18] Koopmans B, Ruigrok J J M, Longa F D and De Jonge W J M 2005 Unifying ultrafast magnetization dynamics *Phys. Rev. Lett.* **95** 267207

[19] Kirilyuk A, Kimel A V and Rasing T 2010 Ultrafast optical manipulation of magnetic order *Rev. Mod. Phys.* **82** 2731–84

[20] Stöhr J and Siegmann H C 2007 *Magnetism: From Fundamentals to Nanoscale Dynamics* (Berlin: Springer)

[21] Tudosa I *et al* 2004 The ultimate speed of magnetic switching in granular recording media *Nature* **428** 831

[22] Gamble S J, Burkhardt M H, Kashuba A, Allenspach R, Parkin S S P, Siegmann H C and Stöhr J 2009 Electric field induced magnetic anisotropy in a ferromagnet *Phys. Rev. Lett.* **102** 217201

[23] Liu M *et al* 2012 Terahertz-field-induced insulator-to-metal transition in vanadium dioxide metamaterial *Nature* **487** 345

[24] Iwaszczuk K, Andryieuski A, Lavrinenko A, Zhang X-C and Jepsen P U 2012 Terahertz field enhancement to the mv/cm regime in a tapered parallel plate waveguide *Opt. Express* **20** 8344–55

[25] Bahk Y-M, Han S, Rhie J, Park J, Jeon H, Park N and Kim D-S 2017 Ultimate terahertz field enhancement of single nanoslits *Phys. Rev.* B **95** 075424

[26] Kozina M *et al* 2017 Local terahertz field enhancement for time-resolved x-ray diffraction *Appl. Phys. Lett.* **110** 081106

[27] Mukai Y, Hirori H, Yamamoto T, Kageyama H and Tanaka K 2014 Antiferromagnetic resonance excitation by terahertz magnetic field resonantly enhanced with split ring resonator *Appl. Phys. Lett.* **105** 022410

[28] Mukai Y, Hirori H, Yamamoto T, Kageyama H and Tanaka K 2016 Nonlinear magnetization dynamics of antiferromagnetic spin resonance induced by intense terahertz magnetic field *New J. Phys.* **18** 013045

[29] Polley D, Pancaldi M, Hudl M, Vavassori P, Urazhdin S and Bonetti S 2018 THz-driven demagnetization with perpendicular magnetic anisotropy: towards ultrafast ballistic switching *J. Phys. D: Appl. Phys.* **51** 084001

[30] Qiu H, Kurihara T, Harada H, Kato K, Takano K, Suemoto T, Tani M, Sarukura N, Yoshimura M and Nakajima M 2018 Enhancing terahertz magnetic near field induced by a micro-split-ring resonator with a tapered waveguide *Opt. Lett.* **43** 1658–61

[31] Pendry J B 2000 Negative refraction makes a perfect lens *Phys. Rev. Lett.* **85** 3966–9

[32] Martín-Moreno L, García-Vidal F J, Lezec H J, Pellerin K M, Thio T, Pendry J B and Ebbesen T W 2001 Theory of extraordinary optical transmission through subwavelength hole arrays *Phys. Rev. Lett.* **86** 1114–7

[33] Chen H-T, Padilla W J, Averitt R D, Gossard A C, Highstrete C, Lee M, O'Hara J F and Taylor A J 2008 Electromagnetic metamaterials for terahertz applications *Terahertz Sci. Technol.* **1** 42–50

[34] Polley D, Ganguly A, Barman A and Mitra R K 2013 Polarizing effect of aligned nanoparticles in terahertz frequency region *Opt. Lett.* **38** 2754

[35] Kumar N, Choudhury S, Polley D, Acharya R, Sinha J, Barman A and Mitra R K 2017 Efficient terahertz anti-reflection properties of metallic anti-dot structures *Opt. Lett.* **42** 1764–7

[36] Kozina M *et al* 2017 Local terahertz field enhancement for time-resolved x-ray diffraction *Appl. Phys. Lett.* **110** 081106

[37] Luo H, Hu X, Qiu Y and Zhou P 2014 Design of a wide-band nearly perfect absorber based on multi-resonance with square patch *Solid State Commun.* **188** 5–11

[38] Padilla W J, Taylor A J, Highstrete C, Lee M and Averitt R D 2006 Dynamical electric and magnetic metamaterial response at terahertz frequencies *Phys. Rev. Lett.* **96** 107401

[39] Kumar N, Strikwerda A C, Fan K, Zhang X, Averitt R D, Planken P C M and Adam A J L 2012 THz near-field Faraday imaging in hybrid metamaterials *Opt. Express* **20** 11277

[40] Liu Z, Huang C-Y, Liu H, Zhang X and Lee C 2013 Resonance enhancement of terahertz metamaterials by liquid crystals/indium tin oxide interfaces *Opt. Express* **21** 6519–6525

[41] COMSOL Multiphysics ® v. 5.2. COMSOL AB, Stockholm, Sweden

[42] Naftaly M and Miles R E 2007 Terahertz time-domain spectroscopy for material characterization *Proc. IEEE* **95** 1658–65

[43] Wen Q-Y, Zhang H-W, Xie Y-S, Yang Q-H and Liu Y-L 2009 Dual band terahertz metamaterial absorber: design, fabrication, and characterization *Appl. Phys. Lett.* **95** 241111

[44] Jackson J D 1999 *Classical Electrodynamics* 3rd edn (New York: Wiley)

[45] Hoffmann M C, Yeh K-L, Hebling J and Nelson K 2007 Efficient terahertz generation by optical rectification at 1035 nm *Opt. Express* **15** 11706–13
[46] Brunner F D J, Kwon O-P, Kwon S-J, Jazbinšek M, Schneider A and Günter P 2008 A hydrogen-bonded organic nonlinear optical crystal for high-efficiency terahertz generation and detection *Opt. Express* **16** 16496–508
[47] Seo M A *et al* 2009 Terahertz field enhancement by a metallic nano slit operating beyond the skin-depth limit *Nat. Photon.* **3** 152
[48] Hoffmann M C, Schulz S, Wesch S, Wunderlich S, Cavalleri A and Schmidt B 2011 Coherent single-cycle pulses with mv/cm field strengths from a relativistic transition radiation light source *Opt. Lett.* **36** 4473–5
[49] Uhd Jepsen P, Cooke D G and Koch M 2011 Terahertz spectroscopy and imaging-modern techniques and applications *Laser Photonics Rev.* **5** 124–66
[50] Koschny T, Markoš P, Smith D R and Soukoulis C M 2003 Resonant and antiresonant frequency dependence of the effective parameters of metamaterials *Phys. Rev.* E **68** 065602
[51] Baena J D, Marqués R, Medina F and Martel J 2004 Artificial magnetic metamaterial design by using spiral resonators *Phys. Rev.* B **69** 014402
[52] Johnson N P, Khokhar A Z, Chong H M, De La Rue R M, Antosiewicz T J and McMeekin S 2006 A review of size and geometrical factors influencing resonant frequencies in metamaterials *Opto-Electron. Rev.* **14** 187
[53] Terman F E 1943 *Radio Engineers' Handbook* (New York: McGraw-Hill)
[54] Knight D W 2016 *The self-resonance and self-capacitance of solenoid coils-applicable theory models and calculation methods* (https://doi.org/DOI: 10.13140/RG.2.1.1472.0887)
[55] Pancaldi M, Freeman R, Hudl M, Hoffmann M C, Urazhdin S, Vavassori P and Bonetti S 2018 Anti-reflection coating design for metallic terahertz meta-materials *Opt. Express* **26** 2917–27
[56] Lee Y-S, Meade T, Perlin V, Winful H, Norris T B and Galvanauskas A 2000 Generation of narrow-band terahertz radiation via optical rectification of femtosecond pulses in periodically poled lithium niobate *Appl. Phys. Lett.* **76** 2505–7
[57] Shi W and Ding Y J 2003 Continuously tunable and coherent terahertz radiation by means of phase-matched difference-frequency generation in zinc germanium phosphide *Appl. Phys. Lett.* **83** 848–50
[58] Chen Z, Zhou X, Werley C A and Nelson K A 2011 Generation of high power tunable multicycle teraherz pulses *Appl. Phys. Lett.* **99** 071102
[59] Carbajo S, Schulte J, Wu X, Ravi K, Schimpf D N and Kärtner F X 2015 Efficient narrowband terahertz generation in cryogenically cooled periodically poled lithium niobate *Opt. Lett.* **40** 5762–5
[60] Stojanovic N and Drescher M 2013 Accelerator-and laser-based sources of high-field terahertz pulses *J. Phys. B: At. Mol. Opt. Phys.* **46** 192001
[61] Green B *et al* 2016 High-field high-repetition-rate sources for the coherent thz control of matter *Sci. Rep.* **6** 22256